Integrated Assessment
2003, Vol. 4, No. 4, pp. 265–282

Taylor & Francis
Taylor & Francis Group

An Inverse Approach to the Analysis of Uncertainty in Models of Environmental Systems

O.O. OSIDELE* AND M.B. BECK

Environmental Informatics and Control Program, Warnell School of Forest Resources, University of Georgia, Athens, GA 30602, USA

ABSTRACT

An inverse methodology that integrates qualitative and quantitative aspects of uncertainty in environmental modeling is presented. The methodology, RIMME (Random-search Inverse Methodology for Model Evaluation), comprises three Monte Carlo procedures: (i) Regionalized Sensitivity Analysis (RSA); (ii) Tree-Structured Density Estimation (TSDE); and (iii) Uniform Covering by Probabilistic Rejection (UCPR). Unlike conventional direct predictive approaches, inverse methods work backwards to identify attributes of the model, and the corresponding real system, that are critical to attaining a prescribed endpoint. RIMME is capable of integrating scientific uncertainties, in the model and empirical data, with non-standard, qualitative forms of uncertainty, such as the value-laden policy and stakeholder issues that feature prominently in contemporary environmental assessments. RIMME is applied to a case study of Lake Lanier, Georgia (USA), a key resource whose water quality and ecological integrity is perceived by society to now be threatened by rapid urbanization within and around its watershed. Results indicate that RIMME provides an effective bridge across the gap between traditional science and the now emerging post-normal science era.

Keywords: environmental models, integrated methodology, Lake Lanier, Monte Carlo, RIMME, uncertainty.

1. INTRODUCTION

Conventionally, uncertainty analysis in environmental modeling is driven essentially by a *forward-reasoning* process which, for a given problem situation, follows the critical path of: (i) constructing and calibrating a model of the system of interest; (ii) defining a number of optional solution strategies; (iii) using model simulation to shortlist candidate solutions; (iv) using model-based optimization to select the best solution strategy; and (v) using the model to predict the outcome of the selected strategy. This last step includes the analysis of prediction uncertainty, which then informs decision-making and management actions to restore or maintain the desired environmental quality. While the literature is replete with its applications to a broad range of environmental problems (see, for example, the case studies in [1]), the foregoing approach is not without its shortcomings, especially in the handling of uncertainty.

The quality of model-based predictions is often judged primarily by how accurately the constituent parameters are estimated during the prior calibration stage. In other words, prediction uncertainty is typically attributed mainly to parameter uncertainty, and much less to structural and data uncertainties. Data uncertainties are inevitable, not only because of human and instrumentation errors, but also due to the sheer scale of the environmental problems that have emerged in recent times. For instance, the ecological impacts on Lake Lanier of rapid urbanization in its watershed [2], the equitable allocation of the water resources of the Apalachicola, Chattahoochee, and Flint river basins among the neighboring states of Alabama, Georgia, and Florida in the United States [3], and the global impacts of humans on climate change, and vice versa [4], are typical examples of the issues now being addressed with the aid of simulation models. However, the currently available empirical data are inadequate, both in quality and quantity, to rigorously assess such large and complex models and, as a result, their predictions are often grossly uncertain. Structural uncertainty is a poorly understood, yet inadequately researched, and often controversial aspect of model evaluation (see the discussion of [5]). Parameters are attributes of a given choice of model structure. Thus, parameter uncertainty derives its meaning only within the context of the model structure under consideration. For this reason, structural uncertainty is typically analyzed and expressed in terms of parameter uncertainty, which always invokes questions about uncertainty in the choice of the model structure itself. A model structure is selected based on existing theoretical paradigms

*Address correspondence to: O.O. Osidele, CNWRA, Southwest Research Institute, P.O. Drawer 28510, San Antonio, TX 78228-0510, USA.

10.1080/13895170490515 41$16.00

and available empirical data, and sometimes, on experience and intuition. The fact that a choice is made among alternative model structures already introduces uncertainty that often may not be elucidated by formal quantitative methods. Nonetheless, promising insights have emerged from recent studies on methodologies for model structure evaluation (for example, [5–9]). Two other sources of uncertainty deserve more focus [10]: (i) the future temporal pattern of variation of forcing functions and external inputs to the system; and (ii) the estimated initial state of the system at the start of the prediction. These are sometimes called scenario uncertainties. Future external stressors are predicated upon future events that cannot be anticipated well in advance. Initial states are measured directly, or estimated from prior models. The errors and uncertainties associated with estimating stressors and initial states often contribute substantially to model prediction uncertainty.

Yet, uncertainty is not limited to the model, data, and scenarios, but includes several qualitative and practical issues, such as, model suitability to the problem context, its influence on policy-making, model development practices, conceptual assumptions, ease of use, and access to technical support [11]. Such issues potentially undermine the credibility of integrated assessment models, and cannot be assessed quantitatively. In an attempt to resolve this inadequacy, the NUSAP method (Numerical Unit Spread Assessment Pedigree) was developed and has been successfully applied to the evaluation of uncertainties in a global energy model [12].

This study explores uncertainty analysis in the context of a *backward-reasoning* process, intended to complement, rather than substitute, the traditional forward-reasoning process. Based on a novel concept of *adaptive community learning*, implemented as an iterative process for generating environmental foresight [2, 13], backward-reasoning follows a critical path of: (i) eliciting stakeholder concerns for the future state of the environment; (ii) encoding the science base in the form of a mathematical simulation model; (iii) using the model to evaluate the plausibility of the stakeholder-derived endpoints of step (i); (iv) communicating the results back to the stakeholders; and (v) feedback from the stakeholders, in the form of revised outlooks for the future, which returns the process back to step (i) for another iteration. In this process, the science base is also enhanced, as subsequent iterations progressively identify the critical scientific uncertainties that are most relevant to the stakeholders' concerns. In essence, the process uses target endpoints to evaluate the model's predictive capabilities, and the *backcasting* of such endpoints to reveal key unknowns and direct the focus of scientific research on the environmental system. Inclusion of stakeholders in the uncertainty evaluation process invites the need to deal with ambiguities in value judgment and human imagination, here expressed qualitatively by the several different endpoints speculated by individual stakeholders. Indeed, this is the essence of an emerging *post-normal science* era that features equitable participation between scientists and stakeholders in decision-making on science-related issues [14, 15].

In what follows, an inverse approach to uncertainty analysis is described and applied to a case study of the multipurpose Lake Lanier, the single most important water resource in the state of Georgia, USA, and the focus of recent studies on the long-term ecological integrity of rapidly developing urban watersheds [2]. The goal of this preliminary assessment is to answer two questions of uncertainty: (i) *to what extent are the imagined future endpoints plausible*?; and (ii) *what are the key scientific uncertainties that determine their plausibility*? To this end, computational analysis of uncertainty is implemented by a recently developed inverse methodology, called RIMME (Random-search Inverse Methodology for Model Evaluation), that integrates three Monte Carlo procedures [16]: univariate Regionalized Sensitivity Analysis (RSA; [17]), extended by multivariate Tree Structured Density Estimation (TSDE; [18]), and augmented with a Uniform Covering by Probabilistic Rejection (UCPR; [19]) sampling procedure. These procedures still conform to the traditional parameter-centric approach to model evaluation, and indeed share a common ancestry with several other Monte Carlo-based methods, such as Generalized Likelihood Uncertainty Estimation (GLUE; [20]), Bayesian Monte Carlo [21], and Markov Chain Monte Carlo [22]. This study does not evaluate structural uncertainty, but rather, employs a single model structure derived from generally accepted ecological theory and well-known principles of system dynamics. The analysis will also incorporate scenario uncertainties arising from variations in the forcing functions, and from errors in estimating the initial state of the system. Specifically, the temporal patterns of forcing functions and the initial states will be parameterized and combined with the conventional process parameters of the simulation model.

2. THE *RIMME* METHODOLOGY

Uncertainty is often measured as a probability, especially when dealing with empirical quantities [23]. Sampling is therefore an obvious approach to the analysis of uncertainty. Monte Carlo simulation, the simplest and most common sampling-based method, forms the basis of the three procedures that constitute RIMME.

2.1. Regionalized Sensitivity Analysis (RSA)

The goal of RSA is to discriminate *key* from *redundant* uncertainties in the model's parameterizations, in order to identify which constituent processes play a critical role in matching a qualitative definition of behavior of the system of interest. In perhaps the earliest landmark application of the Monte Carlo technique to environmental problems, the RSA procedure was developed in the late 1970s, and employed to

provide direction for research on the (then) poorly understood ecological system of the Peel Inlet estuary, in Southwestern Australia [17, 24]. The focus then, was on cultural eutrophication attributed to the excessive growth of the nuisance alga *Cladophora aff. battersii*. Recently, the RSA procedure has been applied to model structure identification of a reservoir ecosystem in the southeastern United States [8].

In principle, RSA employs the parameters of the model as surrogates for the processes (the constituent hypotheses) they describe in the model's functional representations. Thus, a key system process is identified by the sensitivity of its respective parameter(s) in the model. The procedure involves two fundamental tasks: (i) a qualitative definition of system behavior, and (ii) a binary classification of model outputs. The behavior definition includes a set of thresholds, ceilings, and time bounds derived from available information about the system, which may include empirical data, descriptive observations, or even, informed speculations. These qualitative definitions are composed into a set of constraints that depict a *corridor* of uncertainty through which the model output trajectory must pass in order to qualify as an acceptable simulation of system behavior. Thus, the behavior definitions provide the (uncertainty-laden) task specification for evaluating model output, analogous to the (error-prone) empirical data used in conventional model calibration. However, *sensitivity* in the RSA procedure is conditioned on the behavior definitions, in the form of a binary classification scheme that qualifies a simulation as exhibiting either *behavior* (*B*), if the model outputs fall within the defined constraints, or *nonbehavior* (*NB*), if otherwise.

A range of values is defined for each of p model parameters α_k, $1 \le k \le p$, to reflect the uncertainty in the parameters. Monte Carlo simulation is performed on the model, using vectors sampled from a joint distribution defined over the range of parameter values. The simulation outputs are classified as either *B* or *NB* simulations for the respective candidate parameter vectors, leading to a set of binary elements that indicate which simulations produce the defined behavior, and which do not. Thus, for each parameter, two sets of values are distinguished: $\{\alpha_k|B\}$ in the behavior simulations, and $\{\alpha_k|NB\}$ in the nonbehavior simulations. Next, the Kolmogorov-Smirnov two-sample test (two-sided version) is performed on each parameter, to determine whether its *B* and *NB* values come from *different* statistical populations. The hypothesis test is stated formally as follows [25]:

$$\begin{aligned} H_0&: f_m(\alpha_k|B) = f_n(\alpha_k|NB) \\ H_1&: f_m(\alpha_k|B) \neq f_n(\alpha_k|NB) \\ \textit{Test statistic}&: d_{m,n}(\alpha_k) = \sup_X \|F_m(\alpha_k|B) - F_n(\alpha_k|NB)\| \end{aligned} \tag{1}$$

where $F_m(\alpha_k|B)$ and $F_n(\alpha_k|NB)$ are the sample marginal distribution functions for m behaviors and n nonbehaviors; $f_m(\alpha_k|B)$ and $f_n(\alpha_k|NB)$ are the respective marginal probability density functions; the $\sup_X$ notation, defined as the *supremum* over all X (X, being any set of numbers), refers to the largest vertical separation between the two distribution functions. The rejection rule is expressed as follows: *at what statistical significance level does the computed value of* $d_{m,n}$ *determine the rejection of* H_0? According to the Kolmogorov-Smirnov distribution, a high $d_{m,n}$ value generally implies a low significance level for any given values of m and n, and vice versa.

The importance of the uncertainty in each parameter, and by extension, the role of its respective process in matching the behavior definition, is inversely related to this significance level. A low significance level (i.e., a high $d_{m,n}$ value) means there is a significant difference between the distributions of $\{\alpha_k|B\}$ and $\{\alpha_k|NB\}$, suggesting a sensitive parameter, which indicates a key system process. On the other hand, a high significance level (i.e., a low $d_{m,n}$ value) supports H_0, and indicates a redundant parameter and process; in other words, any value within the predefined range is as likely to succeed, as it is to fail, in matching the behavior definition. Finally, the parameters are ranked in descending order of their respective $d_{m,n}$ values, and conveniently grouped into three sensitivity classes, based on the significance level, as: [*1*] critical, [*2*] important, and [*3*] insignificant.

2.2. Tree-Structured Density Estimation (TSDE)

The aim of the TSDE procedure is to split the parameter domain into a number of high- and low-density subdomains, using estimates of the joint probability density function of the behavior-giving parameters $\{\alpha_k|B\}$ derived from the prior RSA procedure. Spear et al. [18] reviewed their experiences with the RSA procedure, and identified two fundamental weaknesses. First, the *success rate*, i.e., the fraction of behavior (*B*) simulations obtained from the Monte Carlo simulation, hardly exceeded 5% for large models with 20 or more parameters. Thus, RSA often lacked sufficient statistical power to credibly evaluate the difference between the behavior and nonbehavior simulations. The second issue concerned the correlation structures and the region occupied by the *B* parameters within the parameter domain. Whereas, the condition $f_m(\alpha_k|B) \neq f_n(\alpha_k|NB)$, i.e., a significant difference between the distributions of *B* and *NB* parameter values (Equation 1), is sufficient to confirm parameter sensitivity, Spear and Hornberger [17] argue that the converse is not true, because any covariance structure induced under the binary classification cannot be identified by the univariate $d_{m,n}$ test statistic alone. To elaborate on this argument, some model parameters that are combined as products or quotients in process functions may compensate numerically for one another over their respective sampling domains in order to match the behavior definition, thus exhibiting somewhat flattened marginal distributions in $f(\alpha_k|B)$ and $f(\alpha_k|NB)$ that therefore do not clearly distinguish between the *B* and *NB* values in the RSA procedure. Thus, a

parameter ranked as insignificant (Class 3), on the basis of the $d_{m,n}$ test statistic only, is not sufficient to classify its related process likewise.

The foregoing led to an exploration of the Classification And Regression Trees (CART) techniques [26], an effort that culminated in a novel Tree-Structured Density Estimation (TSDE) method for multivariate analysis of the posterior B parameter distributions. The TSDE technique emulates the procedure for constructing a histogram, except that it employs a sequence of recursive *binary splits* to partition the parameter domain into sub-domains with approximately uniform density, consisting of small regions of relatively high-density, and larger sparsely populated regions. These sub-domains are similar, respectively, to the peaks and tails (or troughs) of a histogram. Thus, TSDE addresses the second fundamental weakness of the RSA procedure, by way of a multivariate analysis directed at revealing possible correlation structures among the model parameters.

The TSDE algorithm is as follows. The m behavior-giving parameter vectors $\{\alpha|B\}$ are treated as samples from a population with unknown probability density function $f(\alpha|B)$. The task is to construct a good local approximation $f_1(\alpha|B)$ at any point within the p-dimensional parameter sampling domain D. The relative density for a sub-domain S_j, $1 \leq j \leq d$, d, and its estimation error (L) are calculated as [18]:

$$f_1^{(i)}(\alpha|B) = \frac{m_j}{m} \cdot \frac{1}{S_j} \tag{2a}$$

$$L^{(i)} = -\sum_{j=1}^{d} \left(f_1^{(i)}(\alpha|B)\right)^2 \cdot S_j \tag{2b}$$

where m_j is the number of B parameter vectors in S_j, d the number of sub-domains, and i the iteration index. The first density estimate $f_1^{(0)}$, i.e., for the entire parameter domain, is $1/D$, and thus, $L^{(0)}$ is $-(1/D)$. The sub-domains are constructed by successive binary splits on the axis of the parameter which produces the largest increase in overall accuracy of the density estimate for the multivariate distribution. This identifies the key parameter at every stage of the recursion. To determine how to split a domain, the range for each parameter (i.e., on each axis of the p-dimensional parameter hyperspace) is divided into q equal bins, and the grid points are used as trial splits of the parameter domain; hence, there will be $(p \cdot q)$ different ways to make a split. For each trial split, $(L^{(0)} - L^{(1)})$ measures the increase in accuracy of the density estimate. Thus, the TSDE searches for the optimal split that maximizes $(L^{(0)} - L^{(1)})$. The splitting process is repeated on each of the two newly created sub-domains until one of the following convergence criteria is reached: (i) the maximum increase in accuracy produced by the next set of trial splits is insignificant, or (ii) the sample size in each sub-domain is smaller than some critical number.

The result is a *binary* (inverted) tree structure, as depicted in Figure 1, in which the root node represents the original sampling domain, the other nodes are sub-domains, and the branches (the splits) are determined by the key parameters. The tree ends in several terminal nodes, the final partitions of the original parameter sampling domain, consisting of small densely populated, and larger sparsely populated regions. The *high-density terminal nodes* (HDTN) indicate those regions of the parameter space with high probabilities of matching the behavior definitions. Three useful inferences can be made by examining the TSDE tree. First, the combined *volume* of the HDTNs, expressed as a percentage of the total sampling domain volume, indicates the probability of matching the specified behavior definition. Second, the number of high-density terminal nodes that each parameter defines indicates the relative importance of its role in matching the behavior definition. In general, the higher up a parameter is in the tree, the more critical is its role. Third, tracing down to each HDTN reveals the key parameters that collectively interact to match the behavior definition, thereby illustrating, graphically and qualitatively, the multivariate correlation structures among the behavior-giving parameter values. By extension, therefore, the key process interactions in the real system can also be identified.

2.3. Uniform Covering by Probabilistic Rejection (UCPR)

The UCPR procedure was originally presented as a full-fledged parameter estimation and uncertainty analysis technique for application to ecological models [19]. However, within RIMME, the efficient sampling routine of UCPR provides a means for enhancing the statistical power of RSA by improving the success rate of the Monte Carlo simulation, thus addressing the first fundamental weakness of the RSA procedure. In essence, UCPR systematically searches the parameter domain for those values that produce B simulations.

The UCPR algorithm starts with a stored sample of v parameter vectors that define a sub-region $S_v^{(i)}$ (see Fig. 2), where i is the iteration index. Trial vectors are randomly generated in succession within and around $S_v^{(i)}$. However, the trial model simulation is executed *only* if the trial vector is sufficiently *close* to $S_v^{(i)}$. The closeness is determined as a fraction c of the average nearest-neighbor (euclidian) distance $r_v^{(i)}$ between points in $S_v^{(i)}$, where c is chosen such that the likelihood of generating a trial point farther than $(c \cdot r_v^{(i)})$ from $S_v^{(i)}$ is low (say, 1% or 5%). The sub-region defined by $(c \cdot r_v^{(i)})$ is shown as $R_v^{(i)}$ in Figure 2. The trial vector is substituted into $S_v^{(i)}$ if its corresponding model simulation produces a better fit to the data (in this case, the behavior definition) than the worst-fitting member of $S_v^{(i)}$.

UCPR resembles Markov Chain Monte Carlo [27, 28], in that both methods employ a trial and rejection sampling approach for updating the distribution of parameter vectors. In the so-called Metropolis algorithm, the next state of the Markov chain is chosen by considering a small change to the current state, and then accepting or rejecting the change after

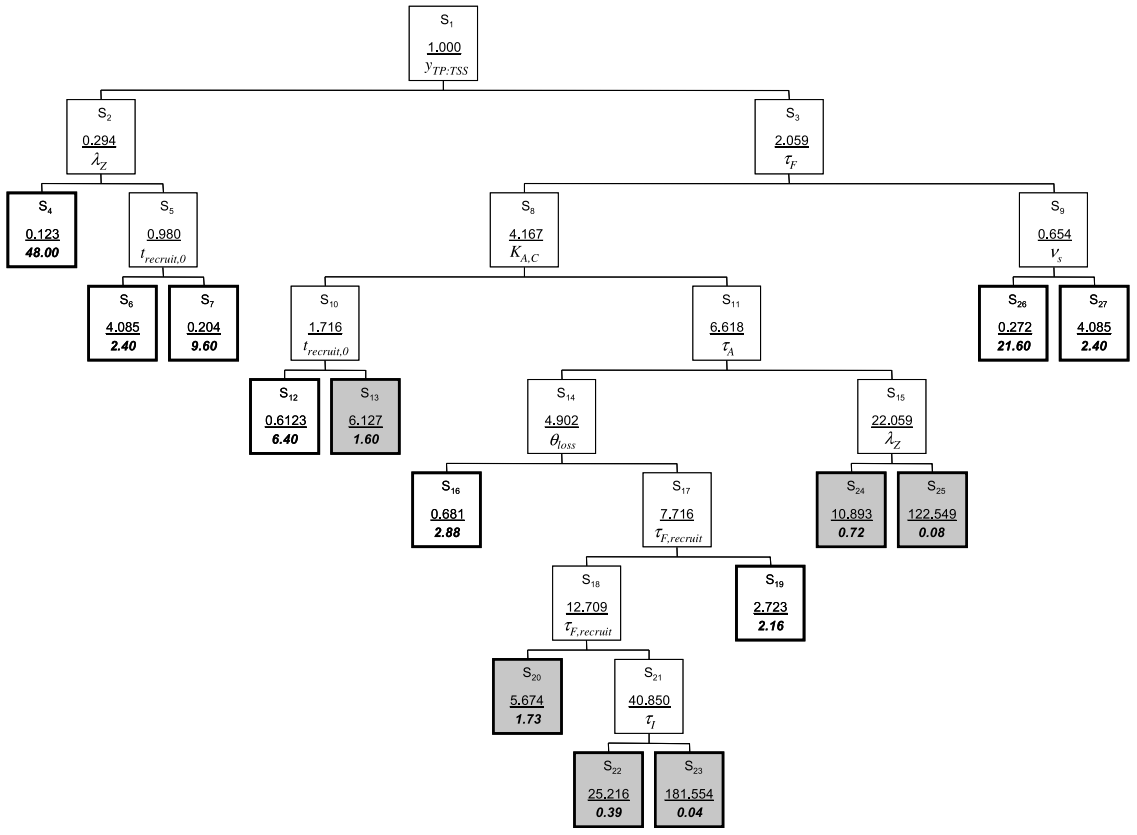

Fig. 1. Example of TSDE tree diagram. High-density terminal nodes are shaded. Node legend: 1st line – node number; 2nd line – relative density of points in the node; 3rd line – input factor that splits intermediate node, or, percentage volume of terminal node.

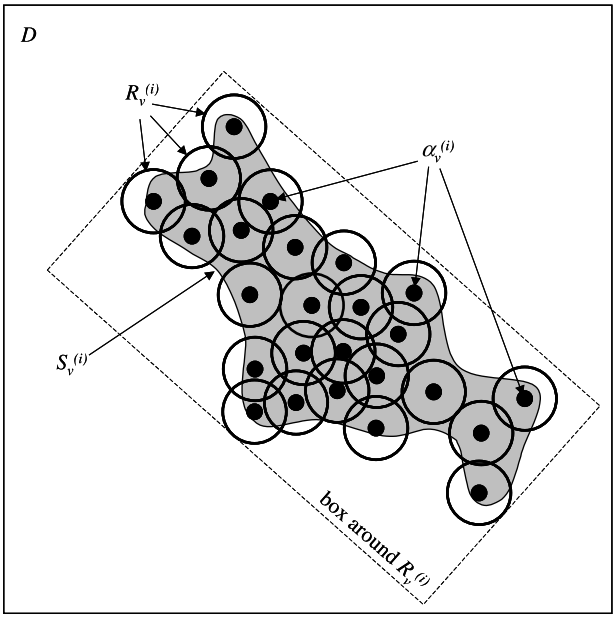

Fig. 2. The UCPR algorithm, depicted on a 2-dimensional sampling domain (D). For each iteration (i), $\alpha_v^{(i)}$ are parameter vectors defining points in D; sub-domain $S_v^{(i)}$ contains the best fitting points; $R_v^{(i)}$ approximates $S_v^{(i)}$ with an aggregate of circles of radius $(c \cdot r_v^{(i)})$ around each point; trial points are generated uniformly in the box around $R_v^{(i)}$.

comparing the probabilities of the current and altered states. In UCPR, rejection of the trial parameter vector is based on: (i) its closeness (distance-wise) to the current distribution of vectors, and (ii) its ability to better simulate system behavior than any of the current vectors. UCPR is quite efficient in locating behavior-giving parameter vectors, since it calls the model less frequently. Indeed, it affords a controlled search of the parameter domain D. With each subsequent iteration (i), the value of r_v changes with the *shape* and *volume* of S_v, which either converges on the behavior-giving parameters within $S_v^{(i)}$, or migrates beyond $S_v^{(i)}$ to locate other such regions of the parameter sampling domain. Locating the various regions of behavior-giving parameter values facilitates a global assessment of parameter uncertainty. In the evaluation of a nonlinear toxicological model, Klepper and Bedaux [29] employed UCPR to demonstrate how extant parametric methods, which often assume *a priori* asymptotic normal parameter distributions, could lead to substantial errors in estimating parameter confidence intervals.

2.4. Synthesis of RIMME

RIMME takes advantage of the strengths of its component procedures. Through the behavior definitions, RSA utilizes a variety of expressions that describe several attributes of the

system, for example: (i) total production of selected biotic components of an ecosystem, (ii) average concentrations of chemical constituents of an aquatic system; and (iii) maxima, minima, and duration of specific hydrologic and geologic events. Such attributes typically feature in most empirical and casual observations of the natural environment. In the seminal work of Hornberger and Spear [24], the behavior definitions were derived from empirical observations. Numerical data from previous studies on the Peel Inlet (Australia) were translated directly into a set of intervals, each defining the range of values for the state variables of the model. Thus, uncertainty due to data error was included in the evaluation of model outputs. By the same token, therefore, it should not be hard to imagine that multiple casual observations, especially by scientifically lay persons, could also be translated, albeit indirectly, into a set of numerical intervals. Thus, in employing such subjective information, non-standard forms of uncertainty are incorporated into the analysis of model outputs.

In the following case study of Lake Lanier, RSA is conducted on a generalized aquatic food web model to derive a sensitivity-based ranking of the constituent reservoir ecological processes. The analysis is conditioned on stakeholder-derived behavior definitions that describe alternative speculated ecological endpoints. Since RSA is essentially a univariate analysis, the key uncertainties identified by the resulting rankings indicate only single-factor effects, and do not identify process interactions. To address this deficiency, the analysis is expanded by employing the multivariate TSDE procedure for identifying parameter correlation structures, and for estimating the relative feasibility of the alternative ecological endpoints. However, prior application of RSA to a similar model, on a smaller reservoir in the same region as Lake Lanier [8], suggests that Monte Carlo simulation might yield very low success rates. In other words, RSA may not generate a large enough sample size of behavior-giving parameter sets for TSDE to produce credible results. In such a situation, UCPR will precede TSDE in order to search for behavior-giving parameter values within the sampling domain.

Fundamentally, RIMME adopts a Bayesian approach to model uncertainty evaluation. In executing the RSA procedure, a prior joint distribution of parameters, $f(\alpha)$, is updated via Monte Carlo experiments on a simulation model, to produce posterior distributions, $f(\alpha|B)$ and $f(\alpha|NB)$, conditioned on the match and mismatch of model outputs with system behavior definitions. The TSDE procedure further characterizes the correlation structures within $f(\alpha|B)$ by identifying the high-density regions, which could be updated by further simulation experiments. A companion procedure, GLUE [20], is also founded on Bayesian principles. Unlike RSA, which employs a binary (2-set) classification, GLUE adopts an n-set classification of the Monte Carlo simulation outputs. The informing likelihood functions (actually, goodness-of-fit between model output and observational data) are also used as weights to update prior parameter uncertainties before propagation into model prediction uncertainties. In contrast, RSA is more simplistic in the sense that the behavior-giving parameter vectors are treated as equally likely simulators of the real system, and when combined with TSDE, the correlations within the posterior parameter distributions are better described. RIMME, GLUE, and other Monte Carlo methods indeed complement each other in various ways, and their relative benefits often depend on the nature and quality of information available for the system of interest. For example, whereas GLUE is well suited to applications that involve numerical data, RIMME seems to perform better with casual observations and experiential knowledge. The following case study will demonstrate the capabilities of RIMME in situations that integrate stakeholder experience and imagination with conventional scientific theory.

3. CASE STUDY: LAKE LANIER, GEORGIA, USA

Lake Lanier (normal storage: $2.4 \times 10^9\,m^3$; surface area: $150\,km^2$) is one of nine reservoirs built and managed by the United States Army Corps of Engineers in the state of Georgia. It is impounded on the Chattahoochee River by the Buford Dam, about 80 km northeast of Atlanta (Fig. 3), and provides hydropower generation, water supply to Atlanta and parts of North Georgia, flood control and navigation, as well as recreation. It was also the focus of a recent study on the ecological integrity of rapidly urbanizing watersheds [2]. The Lanier study aimed at integrating the social sciences (in

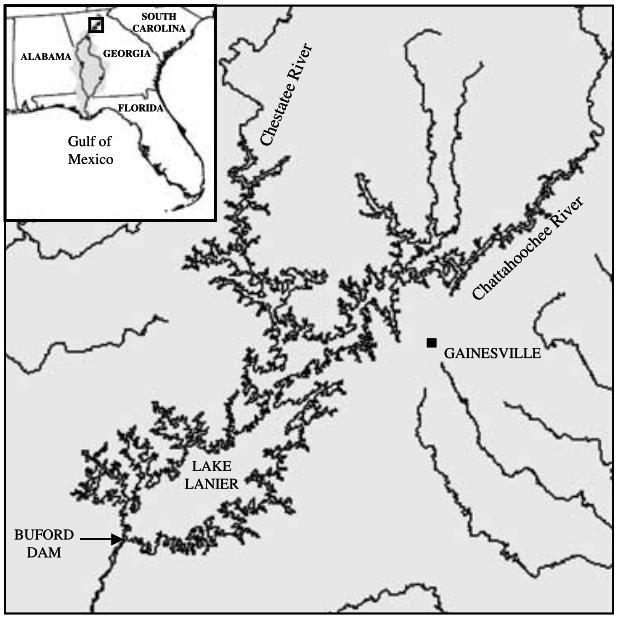

Fig. 3. Location map of Lake Lanier. Inset: the Apalachicola-Chattahoochee-Flint river basin.

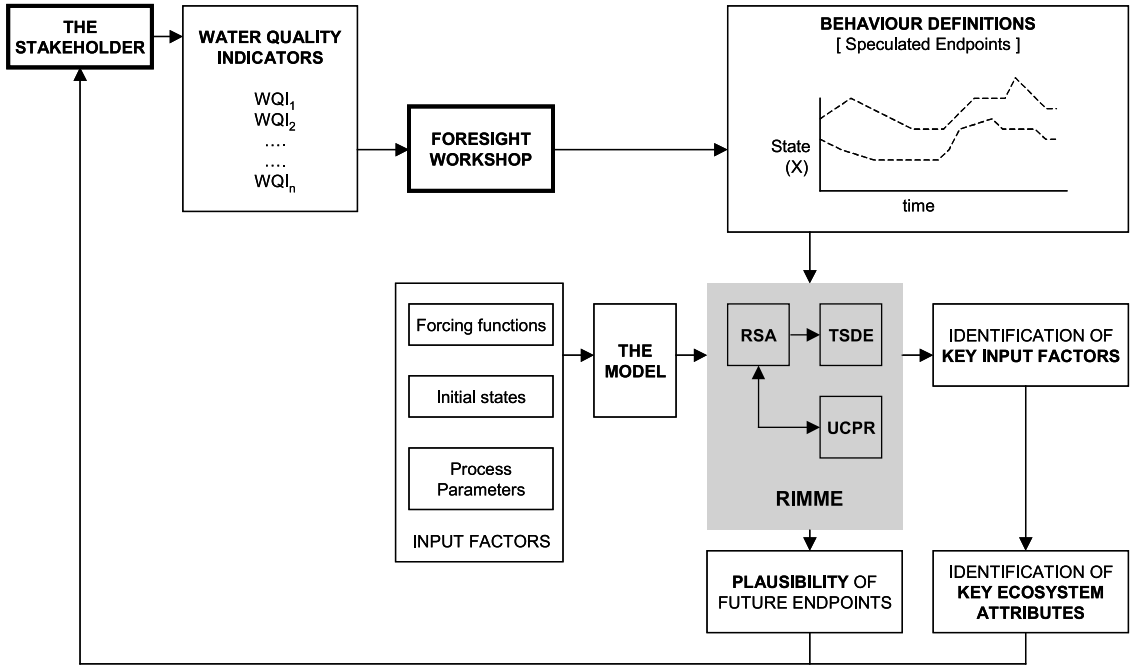

Fig. 4. Schematic representation of the framework for adaptive community learning.

particular, sociology), informed by the concerns of the local community of stakeholders for the future condition of the reservoir and its environs, with the natural sciences of limnology and hydrology, represented by mathematical simulation models. Thus, the concept of adaptive community learning emerged, whereby stakeholder interests direct the focus of scientific research, while science, in return, systematically evaluates the feasibility of stakeholders' concerns for their cherished piece of the environment.

Figure 4 illustrates the procedure for adaptive community learning employed for this study. In this framework, RIMME provides a computational scheme for integrating stakeholder imagination with scientific theory. Stakeholder-derived ecological endpoints, expressed in terms of selected reservoir water quality indicators, are translated into behavior definitions. The RSA procedure, augmented with UCPR sampling, ranks the importance of selected uncertain model input factors (parameters, initial states, and forcing functions), conditioned on the prescribed behavior definitions. This ranking identifies key input factors, from which corresponding key ecosystem attributes (internal ecological processes and external stressors) are derived. In addition, the TSDE procedure estimates the likelihood of attaining the speculated endpoints, given the scientific knowledge encoded in the model. The feedback allows stakeholders to revise their perceptions and endpoints, thus facilitating another iteration through the procedure. As a side-product, the ranking of ecosystem attributes assists scientists in identifying priority areas for future research on the reservoir's ecology.

3.1. The Simulation Model and Input Factors

The model simulates the seasonal dynamics of 13 state variables in the pelagic food web and surface sediment layer of the reservoir ecosystem. The state variables represent functional groups that include biota, soluble reactive phosphorus (SRP), organic matter (detritus), and suspended sediments, linked by physical and trophic interactions. The model integrates three basic ecosystem concepts (see Fig. 5): (i) the classical *grazing* food chain, represented by the pathway: phosphorus → phytoplankton → macrozooplankton → fish; (ii) the *microbial loop*, pathway: detritus → microbes → microzooplankton → macroinvertebrates → fish; and (iii) the release of phosphorus from the surface sediment layer into the water column. Table 1 lists the state variables, forcing functions, and bathymetry constants. In addition, the three sources of model uncertainty adopted as input factors for this analysis (i.e., the process parameters, initial states, and forcing functions) are listed in Tables 2–4. The model equations and parameterization of input factors are detailed in Osidele and Beck [30]. Overall, 94 input factors are analyzed, comprising 57 process parameters, 12 initial conditions, and 25 parameters that describe the temporal pattern of forcing functions.

3.2. The Behavior Definitions

Elicitation of stakeholders' concerns for the future of Lake Lanier was conducted with two experimental devices [2, 31]: a questionnaire survey; and a foresight workshop. The

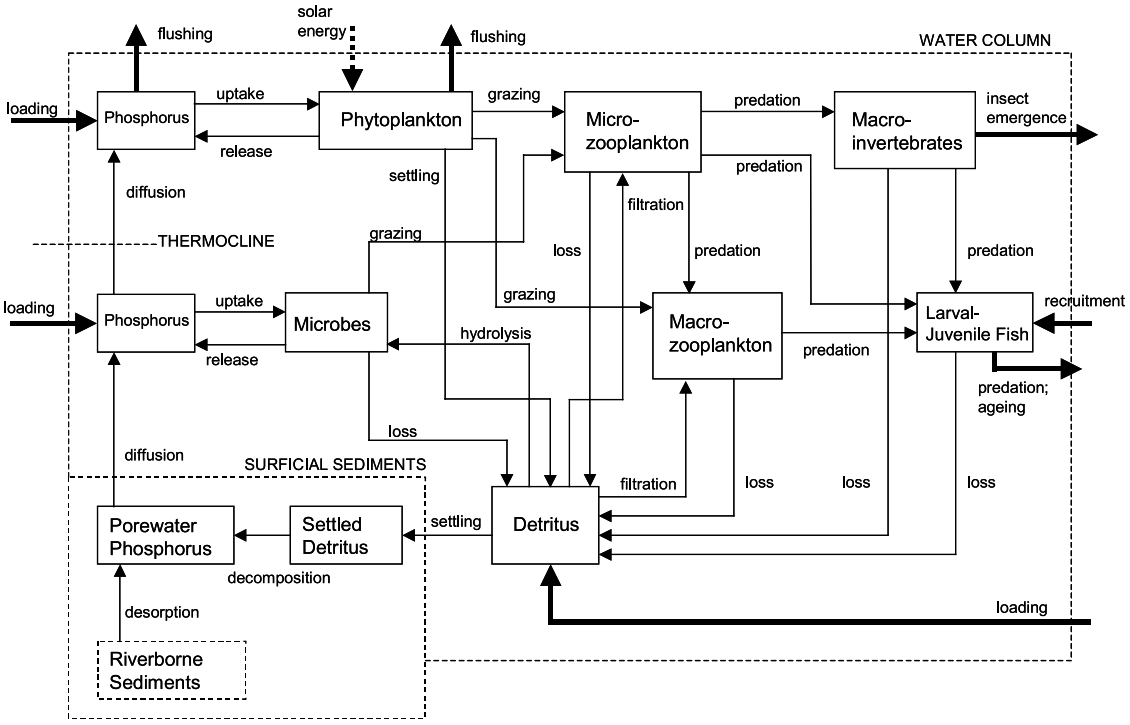

Fig. 5. Schematic representation of the simulation model for Lake Lanier.

Table 1. Features of the Lake Lanier ecological model.

Symbol	Feature	Unit
State variables		
PE	Epilimnion SRP	$\mu g P L^{-1}$
PH	Hypolimnion SRP	$\mu g P L^{-1}$
PS	Dissolved Porewater Phosphorus	$\mu g P L^{-1}$
A	Phytoplankton (as Carbon)	$mg C L^{-1}$
M	Microbes (as Carbon)	$mg C L^{-1}$
H	Microzooplankton	$mg L^{-1}$ dry wt.
C	Macrozooplankton	$mg L^{-1}$ dry wt.
I	Macroinvertebrates	$mg m^{-2}$ dry wt.
F	Larval-Juvenile Fish	$kg ha^{-1}$
DL	Labile Detritus (in water column)	$mg C L^{-1}$
DR	Refractory Detritus (in water column)	$mg C L^{-1}$
DS	Detritus (in sediment layer)	$g C m^{-2}$
TSS	Suspended Solids	$mg m^{-2}$
Forcing functions		
Q_{in}	Upstream inflow	$m^3 s^{-1}$
Q_{out}	Downstream discharge	$m^3 s^{-1}$
L_o	Incident solar radiation	$cal m^{-2} day^{-1}$
T_e	Epilimnion water temperature	°C
T_h	Hypolimnion water temperature	°C
ψ_L	Photoperiod	–
Bathymetry constants		
d_e	Epilimnion depth	m
d_h	Hypolimnion depth	m
V_r	Reservoir volume	m^3
V_e	Epilimnion volume	m^3
V_h	Hypolimnion volume	m^3
A_r	Reservoir surface area	m^2
A_t	Thermocline surface area	m^2

composition of behavior definitions for this analysis is derived solely from the results of the foresight workshop. The workshop was aimed at generating foresight from those who have detailed scientific and experiential knowledge about Lake Lanier [32]. In order to capture the extremes of stakeholder foresight, participants at the workshop were required to speculate on *feared* and *desired* endpoints for the reservoir, and to quantify expected changes in selected reservoir water quality indicators for each endpoint on a predefined logarithmic scale of -10 (one-tenth of the current value) to $+10$ (ten times the current value). Details of the workshop results, and the translation of the speculated changes into system behavior definitions are reported in Cowie et al. [32] and Osidele [16].

Table 5 summarizes the distribution of responses from the participants as quantiles for 10%, 25%, 50% (the median), 75%, and 90%. The medians reflect generally accepted concepts of reservoir limnology. For the feared endpoint, nutrient concentrations (Total Nitrogen and Total Phosphorus) are expected to increase, leading to increased algal production (Chlorophyll a) and a decrease in transparency (Water Clarity). The increased water temperature undermines fish productivity by reducing available habitat (certain prized species often prefer the cooler water in the deeper parts of the reservoir). Higher temperatures also lead to faster rates of respiration and microbial decomposition, which further starve the fish of dissolved oxygen. These directions of change are all reversed for the desired endpoint, as indicated by the signs of the medians. The distributions also reflect uncertainty in the

Table 2. Input factors for the Lake Lanier ecological model[a].

Symbol	Description	Unit	nv	min	max
Process parameters					
τ_A	Max. growth rate: phytoplankton	day^{-1}		1.0	3.0
τ_M	Max. growth rate: microbes	day^{-1}		1.0	5.0
τ_H	Max. growth rate: microzooplankton	day^{-1}		0.1	0.5
τ_C	Max. growth rate: macrozooplankton	day^{-1}		0.05	0.2
τ_I	Max. growth rate: macroinvertebrates	day^{-1}		0.01	0.05
τ_F	Max. growth rate: fish	day^{-1}		0.01	0.05
$K_{PE,A}$	Half-saturation: phos. → phyt.	$mgP\,L^{-1}$		0.001	0.01
$K_{PH,M}$	Half-saturation: phos. → microbes	$mgP\,L^{-1}$		0.0	0.001
$K_{D,M}$	Half-saturation: detritus → microbes	$mgC\,L^{-1}$		0.02	0.15
$K_{A,H}$	Half-saturation: phyt. → microzoop.	$mgC\,L^{-1}$		1.0	10.0
$K_{M,H}$	Half-saturation: microbes → microzoop.	$mgC\,L^{-1}$		0.01	0.05
$K_{D,H}$	Half-saturation: detritus → microzoop.	$mgC\,L^{-1}$		0.01	0.05
$K_{A,C}$	Half-saturation: phyt. → macrozoop.	$mgC\,L^{-1}$		0.1	1.0
$K_{H,C}$	Half-saturation: microzoop. → macrozoop.	$mgdw\,L^{-1}$		1.0	5.0
$K_{D,C}$	Half-saturation: detritus → macrozoop.	$mgC\,L^{-1}$		1.0	10.0
$K_{H,I}$	Half-saturation: microzoop. → macroinv.	$mgdw\,L^{-1}$		1.0	5.0
$K_{D,I}$	Half-saturation: detritus → macroinv.	$mgC\,L^{-1}$		1.0	10.0
$K_{H,F}$	Half-saturation: microzoop. → fish	$mgdw\,L^{-1}$		5.0	10.0
$K_{C,F}$	Half-saturation: macrozoop. → fish	$mgdw\,L^{-1}$		0.05	0.1
$K_{I,F}$	Half-saturation: macroinv. → fish	$mgdw\,m^{-2}$		50.0	200.0
$y_{PE,A}$	Phos. utilization: phyt. Production	$mgP\,mgC^{-1}$	0.03		
$y_{PH,M}$	Phos. utilization: microbial production	$mgP\,mgC^{-1}$	0.05		
$\varepsilon_{D,M}$	Efficiency: detritus → microbes	–		0.3	0.7
$\varepsilon_{A,H}$	Efficiency: phyt. → microzoop.	–		0.05	0.1
$\varepsilon_{M,H}$	Efficiency: microbes → microzoop.	–		0.2	0.5
$\varepsilon_{D,H}$	Efficiency: detritus → microzoop.	–		0.3	0.7
$\varepsilon_{A,C}$	Efficiency: phyt. → macrozoop.	–		0.2	0.5
$\varepsilon_{H,C}$	Efficiency: microzoop. → macrozoop.	–		0.2	0.5
$\varepsilon_{D,C}$	Efficiency: detritus → macrozoop.	–		0.05	0.1
$\varepsilon_{H,I}$	Efficiency: microzoop. → macroinv.	–		0.3	0.7
$\varepsilon_{D,I}$	Efficiency: detritus → macroinv.	–		0.2	0.5
$\varepsilon_{H,F}$	Efficiency: microzoop. → fish	–		0.05	0.1
$\varepsilon_{C,F}$	Efficiency: macrozoop. → fish	–		0.3	0.7
$\varepsilon_{I,F}$	Efficiency: macroinv. → fish	–		0.6	0.9
$y_{TP:TSS}$	TP:TSS ratio in tributary inflow [log10]	–		−3.0	−1.0
y_Z	Zooplankton carbon:biomass ratio	$mgC\,mgdw^{-1}$		0.2	0.7
y_I	Macroinvertebrate carbon:biomass ratio	$mgC\,mgdw^{-1}$	0.5		
y_F	Fish carbon:biomass ratio	$mgC\,mgdw^{-1}$	0.45		
λ_A	Respiration rate: phytoplankton	day^{-1}		0.01	0.05
λ_M	Mortality rate: microbes	day^{-1}		0.5	2.0
λ_Z	Loss rate: zooplankton	day^{-1}		0.01	0.1
λ_I	Loss rate: macroinvertebrates	day^{-1}		0.05	0.1
λ_F	Loss rate: fish	day^{-1}		0.001	0.01

Note. [a]nv, nominal value for input factors excluded from Monte Carlo sampling; [min, max], sampling domain.

overall stakeholder foresight for Lake Lanier. For example, in speculating the desired endpoint, about 80% of the participants (the 10% to 90% quantiles) expect that fish population would increase to between one- and eight-times the current levels. Such uncertainty informs the composition of behavior definitions for this analysis.

The behavior definitions are prescribed in terms of three water quality indicators: (i) soluble reactive phosphorus (SRP) concentration; (ii) Chlorophyll *a* concentration, and (iii) fish biomass. Also, they cover the months of May–September. This is the most critical period of the year for water quality in Lake Lanier, because it coincides with summer stratification, peak primary production, hypolimnetic dissolved oxygen depletion, fish spawning, and the peak recreational season. The resulting behavior definitions are as follows (see Figs. 6 and 7):

Feared endpoint:

- [P]: epilimnion SRP concentration should not exceed $30\,\mu g\,L^{-1}$;
- [U]: mean epilimnion SRP concentration should not exceed $16\,\mu g\,L^{-1}$;
- [P]: Chlorophyll *a* concentration should not exceed $25\,\mu g\,L^{-1}$;

Table 3. Input factors for the Lake Lanier ecological model.

Symbol	Description	Unit	nv	min	max
Process parameters (. . . continued)					
$\tau_{I,emerg}$	Insect emergence rate	day^{-1}		0.001	0.01
$\tau_{F,age}$	Fish ageing rate	day^{-1}		0.01	0.05
$\tau_{G,feed}$	Adult fish feeding rate	day^{-1}		0.002	0.005
$\tau_{F,recruit}$	Fish recruitment rate	day^{-1}		0.002	0.02
$\tau_{dec,s}$	Decomposition rate: in sediment	day^{-1}		0.001	0.01
τ_{des}	Desorption rate: in sediment	day^{-1}		0.001	0.01
$y_{P,dec}$	Phos. yield from decomposition	$mgP\,mgC^{-1}$	0.02		
$y_{P,des}$	Phos. yield from desorption	$mgP\,g^{-1}$	1.5		
s_A	Settling velocity: phytoplankton	$m\,day^{-1}$		0.02	0.06
s_D	Settling velocity: detritus	$m\,day^{-1}$		0.1	0.3
s_{TSS}	Settling velocity: suspended solids	$m\,day^{-1}$		0.1	0.5
θ_{growth}	Temperature coeff.: growth processes	–		1.0	1.1
θ_{loss}	Temperature coeff.: loss processes	–		1.0	1.1
κ_w	Light extinction: clear water	m^{-1}		0.17	0.35
a_A	Light extinction: phyt. Chlorophyll	$L\,(mgC\,m)^{-1}$		0.1	0.6
a_{TSS}	Light extinction: suspended solids	$L\,(mg\,m)^{-1}$		0.01	0.05
L_m	Optimal light intensity: phyt.	$cal\,(m^2\,day)^{-1}$	325		
v_s	Diffusion coeff.: sediment → water [log10]	$m^2\,day^{-1}$		−7.0	0.0
d_s	Effective depth of sediment layer	m		0.01	0.1
ρ_p	Density of sediment solids	$g\,cm^{-3}$	2.5		
ϕ_s	Porosity of sediment layer	–		0.5	0.9
f_{DR}	Proportion of refractory detritus	–		0.0	1.0
G	Adult fish biomass:	$kg\,ha^{-1}$			
	Feared endpoint			18.0	66.0
	Desired endpoint			184.0	1509.0
Initial states					
$PE(0)$	Initial condition: Epilimnion SRP	$\mu gP\,L^{-1}$		1.0	3.0
$PH(0)$	Initial condition: Hypolimnion SRP	$\mu gP\,L^{-1}$		1.0	3.0
$PS(0)$	Initial condition: Sediment Phosphorus	$\mu gP\,L^{-1}$		10.0	50.0
$A(0)$	Initial condition: Phytoplankton	$mgC\,L^{-1}$		0.1	1.5
$M(0)$	Initial condition: Microbes	$mgC\,L^{-1}$		0.1	1.0
$H(0)$	Initial condition: Microzooplankton	$mg\,L^{-1}$ dw.		0.01	0.1
$C(0)$	Initial condition: Macrozooplankton	$mg\,L^{-1}$ dw.		0.01	0.1
$I(0)$	Initial condition: Macroinvertebrates	$mg\,m^{-2}$ dw.		20.0	60.0
$F(0)$	Initial condition: Larval-Juvenile Fish	$kg\,ha^{-1}$	0.0		
$DL(0)$	Initial condition: Labile Detritus	$mgC\,L^{-1}$		0.1	0.5
$DR(0)$	Initial condition: Refractory Detritus	$mgC\,L^{-1}$		0.5	1.5
$DS(0)$	Initial condition: Sediment Detritus	$gC\,m^{-2}$		0.1	0.5
$TSS(0)$	Initial condition: Suspended Solids	$mg\,L^{-1}$		1.0	5.0

- [L–U]: mean Chlorophyll *a* concentration should be between 5–16 $\mu g\,L^{-1}$;
- [L–U]: mean larval-juvenile fish biomass should be between 3–9 $Kg\,ha^{-1}$;

Desired endpoint:

- [P]: epilimnion SRP concentration should not exceed 5 $\mu g\,L^{-1}$;
- [U]: mean epilimnion SRP concentration should not exceed 2 $\mu g\,L^{-1}$;
- [P]: Chlorophyll *a* concentration should not exceed 3 $\mu g\,L^{-1}$;
- [L–U]: mean Chlorophyll *a* concentration should be between 0.4–1.9 $\mu g\,L^{-1}$;
- [L–U]: mean larval-juvenile fish biomass should be between 25–205 $Kg\,ha^{-1}$.

For each endpoint, five RSA replicates are performed, based on 5000 model simulations each. The Monte Carlo samples are obtained from a joint uniform distribution of the input factors defined over the range of values derived from an extensive literature search (Tables 2–4; see also [30]). No other information describing the parameter distributions is available. Data recorded from previous field studies do not include the food web components of the model adopted for this study. Also, due to significant structural differences, it is difficult to adopt parameter estimates from previous model calibrations. The joint uniform distribution therefore provides a reasonable prior distribution for this analysis. This choice indeed reflects the Bayesian approach to statistical analysis [33], in selecting the least informative prior distribution relative to what is expected from the intended experiment. Figures 6 and 7 illustrate examples of the

Table 4. Input factors for the Lake Lanier ecological model.

Symbol	Description	Unit	nv	min	max
External inputs and forcing functions					
N_Q	Index of inflow and discharge time series	–		1	35
N_L	Index of solar radiation time series	–		1	4
$T_{e,avg}$	Mean daily water temperature: epilimnion	°C			
	Feared endpoint			21	27
	Desired endpoint			16	22
$T_{h,avg}$	Mean daily water temperature: hypolimnion	°C		8	12
$\psi_{L,avg}$	Mean daily photoperiod	–	0.5		
$T_{e,rng}$	Range of water temperature: epilimnion	°C		19	21
$T_{h,rng}$	Range of water temperature: hypolimnion	°C		4	6
$\psi_{L,rng}$	Range of photoperiod	–	0.2		
$T_{e,phs}$	Time of mean water temperature: epilimnion	Julian day		135	155
$T_{h,phs}$	Time of mean water temperature: hypolimnion	Julian day		175	195
$\psi_{L,phs}$	Time of mean daily photoperiod	Julian day	78		
$t_{emerg,0}$	Onset of insect emergence	Julian day		75	130
$t_{recruit,0}$	Onset of fish spawning	Julian day		105	165
$t_{emerg,d}$	Duration of insect emergence	day		100	200
$t_{recruit,d}$	Duration of fish spawning	day		30	60
$t_{no\text{-}age,d}$	Duration of no fish ageing	day		50	120
$\nu_{t,mix}$	Diffusion coeff. (thermocline) at full mixis	$m\,day^{-1}$		4	10
$t_{strat,0}$	Onset of stratification	Julian day		90	105
$t_{strat,m}$	Time of stable stratification	Julian day		150	165
$t_{mix,0}$	Onset of destratification	Julian day		300	310
$t_{mix,m}$	Time of full mixis	Julian day		345	355
$f_{PE,ovfl}$	Max. fraction of phosphorus load into epilimnion	–		0.6	1.0
$t_{ovfl,0}$	Onset of transition: underflow → overflow	Julian day		25	35
$t_{ovfl,m}$	Time of stable overflow	Julian day		85	95
$f_{PE,undfl}$	Min. fraction of phosphorus load into epilimnion	–		0.2	0.5
$t_{undfl,0}$	Onset of transition: overflow → underflow	Julian day		180	210
$t_{undfl,m}$	Time of stable underflow	Julian day		270	280

Table 5. Quantiles for the distribution of speculated changes[a].

Water quality indicator	Feared endpoint					Desired endpoint				
[*quantiles*, %] →	10	25	50	75	90	10	25	50	75	90
Total nitrogen	−3.7	2.4	3.7	4.6	6.4	−6.4	−4.2	−2.1	−1.5	1.0
Total phosphorus	3.7	4.6	4.6	6.4	8.2	−4.6	−4.2	−2.8	−2.1	−1.5
Water clarity	−10.0	−6.4	−5.7	−3.3	−2.8	1.5	2.1	2.8	2.8	4.6
Chlorophyll *a*	2.8	4.2	5.5	8.2	8.2	−4.6	−3.9	−2.6	−1.7	1.0
Fish population	−10.0	−8.7	−6.4	−4.6	−2.8	1.0	1.9	2.8	4.6	8.2
Avg. ann. water temperature	70	75	76	76	79	62	64	68	70	70

Note. [a]Speculations for future water temperature are absolute values.

behavior-giving (B) simulations for the feared and desired endpoints respectively, each summarized by envelope and median plots of the model outputs.

3.3. RSA Rankings

Sensitivity classifications (C_S) of input factors for the feared and desired endpoints (see Tables 6 and 7) are based on the following rule: Class 1 (critical) includes the input factors with $d_{m,n}$ values corresponding to a significance level less than 10%; Class 2 (important) contains those between 10% and 20%, inclusive; and Class 3 (insignificant), those greater than 20%. Ranks (r) are assigned to input factors in each replicate, in decreasing order of their respective $d_{m,n}$ values. Finally, the overall top 20 input factors are determined by summing the ranks (Σr) across all five RSA replicates. The top 20 ranks are selected because, on the whole, they contain at least 75% of the critical (Class 1) input factors. However, not all of the overall top 20 input factors appear in the top 20 ranks in every RSA replicate. This suggests the possible existence of correlations among the input factors, whereby the prescribed behavior definitions are matched by several different combinations of key input factors. The high dimensionality of the model (i.e., with 94 uncertain input

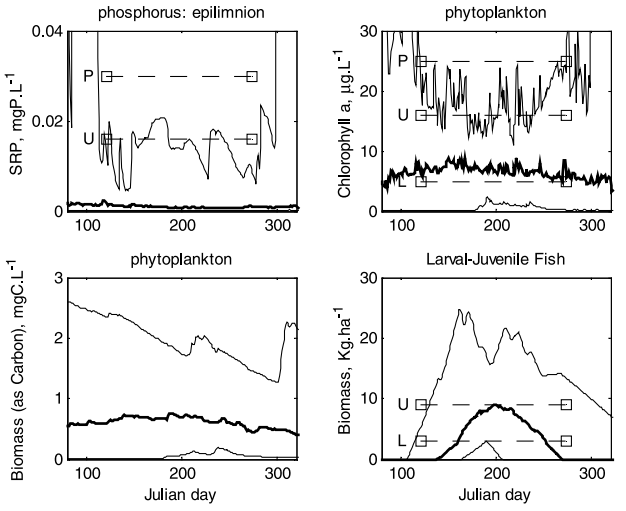

Fig. 6. Example of Monte Carlo simulation for the behavior-giving (B) model outputs for the feared future endpoint, showing: (i) median plots (thick lines); (ii) envelope plots (thin lines); and (iii) the behavior definitions (dashed lines, with labels: [P]eak value, [U]pper and [L]ower bounds; square bocks indicate the period May–September, Julian day 121–273, during which model ouputs are compared to the behavior definitions).

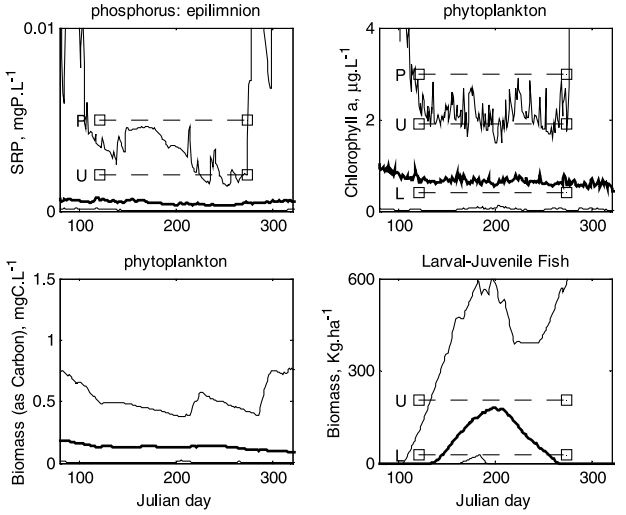

Fig. 7. Example of Monte Carlo simulation for the behavior-giving (B) model outputs for the desired future endpoint, (Legend as in Fig. 6).

factors) further increases the likelihood of correlations among the input factors, which hinders the replicability of results, and potentially undermines the robustness of the results. In this analysis, the five replicates conducted for each endpoint result in different rankings of the input factors. However, a closer inspection of Tables 6 and 7 reveals some consistencies. For example, the overall top four input factors $\{y_{TP:TSS}, \tau_F, \tau_{F,recruit}, \lambda_Z\}$ for the feared endpoint, and the overall top five $\{y_{TP:TSS}, \tau_{F,recruit}, v_s, G, \tau_F\}$ for the desired endpoint, all feature in the top 10 ranks for each RSA replicate. Also, subsequent discussions will show how these and other top tanked input factors collectively describe similar ecological processes across the five replicates. Thus, in spite of the different rankings, the same key macroscopic attributes of the reservoir ecosystem are identified in the RSA replicates.

While Monte Carlo methods, such as RSA, provide an effective means for exploring the entire input factor domain, thereby providing a global analysis of uncertainty for a given problem situation, the sampling involved often raises important issues of replicability and robustness. As discussed above, outcomes of replicate Monte Carlo experiments can be similar yet different in many respects. This is indeed valuable for both the scientist seeking a better understanding of system behavior, and the stakeholder pondering optional policies and actions for improving or maintaining the performance of the system. Whereas the similarities inform the selection of key attributes of the system, the inconsistent outcomes identify different plausible modes of behavior. The challenge to science is often in predicting which of these candidate interpretations will, individually or collectively, determine the eventual future system behavior. In a stakeholder forum, the availability of options widens the scope of deliberations, thus enhancing the quality of decision-making and potentially minimizing the risk of surprise events in the future.

Tables 6 and 7 also show the success rate (m/N) for each RSA replicate, i.e., the proportion of the 5000 simulations that match the behavior definitions. After 5000 model calls, the UCPR sampling routine doubles the sample size of behavior-giving input factors on average across the five replicates for the feared endpoint. The success rates range from 0.98% to 1.10% for the feared endpoint, and from 2.30% to 2.54% for the desired endpoint. This provides merely a hint of the attainability of the speculated endpoints, since success rates do not describe the distributional properties of the behavior-giving input factor values. In general, it would seem that the feared endpoint is less plausible than the desired endpoint, a preliminary inference that might be sufficient to allay the fears of some stakeholders. The low success rates (less than 3%) are a general indication of the extremeness of the speculated endpoints. Perhaps more fundamentally, they could also be attributed to structural inadequacies in the model itself. A common issue with ecological models is the resolution of the constituent state variables and functions. In the model employed for this study (see Fig. 5), spatial segregation is limited to distinguishing the photic, aphotic, and sediment layers in the vertical profile of the reservoir, and taxonomic resolution includes only the macroscopic functional groups of biota and nutrients. However, the process parameters in the same model are often derived from single-species laboratory experiments or microcosm field studies. Thus, the model structure imparts a rather different meaning and scale to the

Table 6. Summary of RSA classification for the feared endpoint[a].

Input factor	Rep. 1			Rep. 2			Rep. 3			Rep. 4			Rep. 5			
	$d_{m,n}$	r	C_s	$d_{m,n}$	r	C_s	$d_{m,n}$	r	C_s	$d_{m,n}$	r	C_s	$d_{m,n}$	r	C_s	Σr
$y_{TP:TSS}$	0.397	(1)	1	0.386	(1)	1	0.470	(1)	1	0.340	(2)	1	0.399	(1)	1	6
τ_F	0.338	(2)	1	0.202	(6)	1	0.350	(2)	1	0.256	(4)	1	0.282	(3)	1	17
$\tau_{F,recruit}$	0.250	(4)	1	0.184	(7)	1	0.286	(3)	1	0.276	(3)	1	0.291	(2)	1	19
λ_Z	0.218	(7)	1	0.222	(5)	1	0.217	(5)	1	0.351	(1)	1	0.270	(4)	1	22
$K_{A,C}$	0.163	(12)	2	0.139	(27)	3	0.284	(4)	1	0.242	(5)	1	0.215	(6)	1	54
τ_C	0.219	(6)	1	0.123	(31)	3	0.200	(7)	1	0.232	(6)	1	0.177	(11)	1	61
$v_{t,mix}$	0.157	(13)	2	0.083	(64)	3	0.175	(9)	1	0.124	(26)	3	0.179	(9)	1	121
v_s	0.098	(41)	3	0.279	(2)	1	0.154	(13)	2	0.131	(25)	3	0.097	(47)	3	128
λ_I	0.109	(32)	3	0.121	(34)	3	0.104	(41)	3	0.172	(11)	2	0.146	(17)	3	135
τ_A	0.151	(18)	2	0.146	(20)	3	0.125	(25)	3	0.092	(54)	3	0.129	(22)	3	139
$\varepsilon_{D,C}$	0.167	(11)	1	0.163	(14)	2	0.116	(33)	3	0.083	(61)	3	0.127	(25)	3	144
a_A	0.229	(5)	1	0.109	(41)	3	0.120	(31)	3	0.057	(83)	3	0.238	(5)	1	165
G	0.129	(24)	3	0.171	(9)	1	0.139	(19)	3	0.086	(59)	3	0.086	(54)	3	165
$\varepsilon_{A,C}$	0.282	(3)	1	0.118	(35)	3	0.082	(62)	3	0.101	(46)	3	0.131	(21)	3	167
y_Z	0.171	(10)	1	0.261	(4)	1	0.055	(86)	3	0.132	(23)	3	0.096	(51)	3	174
τ_I	0.132	(23)	3	0.145	(21)	3	0.082	(61)	3	0.107	(41)	3	0.118	(29)	3	175
$t_{undfl,0}$	0.082	(55)	3	0.137	(28)	3	0.114	(34)	3	0.141	(20)	3	0.110	(38)	3	175
θ_{loss}	0.068	(79)	3	0.122	(33)	3	0.114	(35)	3	0.177	(9)	1	0.136	(20)	3	176
λ_A	0.156	(15)	2	0.123	(32)	3	0.079	(66)	3	0.096	(52)	3	0.157	(13)	2	178
$TSS(0)$	0.102	(35)	3	0.067	(79)	3	0.157	(11)	2	0.119	(31)	3	0.129	(23)	3	179
Pre-UCPR																
m	21			25			19			22			23			
m/N	0.42%			0.50%			0.38%			0.42%			0.46%			
Post-UCPR																
m	55			52			51			50			49			
m/N	1.10%			1.04%			1.02%			1.00%			0.98%			

Note. [a]$d_{m,n}$, Kolmogorov-Smirnov test statistic; C_s, sensitivity class; r, rank; m, number of behavior-giving simulations; N, total number of simulations (5000); m/N, success rate.

process parameters from that of the informing empirical data. For this reason therefore, it is not recommended that the success rates be employed in quantitative assessments, such as in probabilistic risk analysis.

Nevertheless, the resulting distribution of input factors provides some useful insights into the differences in ecological behavior between the stakeholder-derived endpoints. Table 8 lists the medians of the marginal distributions of behavior-giving values for the top 10 input factors in Tables 6 and 7. Five key input factors $\{\tau_F, \lambda_Z, \tau_{F,recruit}, v_s, y_{TP:TSS}\}$ are common to both endpoints. However, the contrast in ranking and distribution for $\{y_{TP:TSS}, v_s, \lambda_Z\}$ is quite significant. First, $\{y_{TP:TSS}\}$, the ratio of total phosphorus to total suspended solids concentration in the tributary inflow, is ranked highest for both endpoints, thus indicating the importance of uncertainties in estimating nutrient loading from the adjoining watershed. However, there is a significant difference in the distribution of this factor, as its median value drops from about 0.8 for the feared endpoint to just 0.4 for the desired endpoint. This outcome agrees with the expectation that at the desired endpoint, which requires less nutrients for reduced primary production, Lake Lanier will receive less nutrient load from its watershed. Second, $\{v_s\}$, the diffusion coefficient representing exchange of soluble phosphorus across the sediment-water interface, is ranked significantly higher for the desired endpoint (and also features in all its five RSA replicates). Against the backdrop of low nutrient concentrations at the desired endpoint, the typically low flux of phosphorus from the sediment layer presumably becomes a key contributor to SRP concentrations in the water column. Third, $\{\lambda_Z\}$, the combined metabolic loss rate constant for micro- and macro-zooplankton drops from fourth place for the feared endpoint, to ninth for the desired endpoint, suggesting that the zooplankton species may play significantly different roles in the aquatic food web at both endpoints, as discussed next.

Indeed, it appears the feared and desired endpoints described by the stakeholders are dominated by two different pathways for energy transfer within the aquatic food web. The food web model integrates the conventional grazing food chain, which includes phytoplankton and macrozooplankton, with the microbial loop, featuring the relatively small-sized microbes and microzooplankton (see Fig. 5). In Table 8, the phytoplankton and macrozooplankton process parameters $\{\tau_A, \tau_C, K_{A,C}\}$ appear in the top 10 ranks for the

Table 7. Summary of RSA classification for the desired endpoint[a].

Input factor	Rep. 1			Rep. 2			Rep. 3			Rep. 4			Rep. 5			
	$d_{m,n}$	r	C_s	$d_{m,n}$	r	C_s	$d_{m,n}$	r	C_s	$d_{m,n}$	r	C_s	$d_{m,n}$	r	C_s	Σr
$y_{TP:TSS}$	0.230	(2)	1	0.275	(1)	1	0.224	(2)	1	0.271	(1)	1	0.245	(1)	1	7
$\tau_{F,recruit}$	0.263	(1)	1	0.250	(2)	1	0.198	(6)	1	0.168	(4)	1	0.205	(2)	1	15
v_s	0.158	(6)	1	0.160	(6)	1	0.198	(4)	1	0.207	(2)	1	0.174	(6)	1	24
G	0.171	(3)	1	0.234	(3)	1	0.200	(3)	1	0.130	(10)	1	0.178	(5)	1	24
τ_F	0.141	(9)	1	0.119	(10)	1	0.284	(1)	1	0.198	(3)	1	0.165	(7)	1	30
τ_H	0.160	(5)	1	0.168	(4)	1	0.108	(16)	2	0.141	(8)	1	0.183	(4)	1	37
τ_M	0.161	(4)	1	0.111	(14)	1	0.198	(5)	1	0.149	(6)	1	0.111	(20)	2	49
λ_M	0.102	(23)	2	0.127	(9)	1	0.141	(11)	1	0.149	(5)	1	0.142	(11)	1	59
λ_Z	0.128	(10)	1	0.164	(5)	1	0.175	(7)	1	0.096	(23)	3	0.071	(38)	3	83
θ_{growth}	0.107	(19)	2	0.062	(53)	3	0.122	(14)	1	0.125	(13)	1	0.151	(8)	1	107
$T_{e,avg}$	0.099	(24)	2	0.099	(19)	2	0.078	(32)	3	0.113	(14)	2	0.116	(19)	1	108
$t_{recruit,d}$	0.082	(32)	3	0.119	(11)	1	0.089	(23)	3	0.069	(39)	3	0.191	(3)	1	108
τ_C	0.122	(15)	1	0.049	(67)	3	0.147	(9)	1	0.130	(12)	1	0.107	(23)	2	126
$t_{no\text{-}age,d}$	0.063	(48)	3	0.086	(25)	3	0.097	(20)	3	0.096	(24)	3	0.142	(10)	1	127
$\tau_{F,age}$	0.103	(22)	2	0.156	(7)	1	0.083	(26)	3	0.068	(45)	3	0.089	(28)	3	128
$T_{h,avg}$	0.080	(36)	3	0.107	(17)	2	0.090	(22)	3	0.061	(51)	3	0.085	(30)	3	156
$t_{strat,m}$	0.074	(39)	3	0.099	(21)	2	0.130	(13)	1	0.057	(58)	3	0.094	(25)	3	156
$\varepsilon_{H,I}$	0.068	(43)	3	0.057	(58)	3	0.149	(8)	1	0.082	(34)	3	0.080	(32)	3	175
N_Q	0.158	(7)	1	0.074	(38)	3	0.056	(57)	3	0.085	(31)	3	0.062	(45)	3	178
τ_{des}	0.044	(73)	3	0.082	(27)	3	0.098	(19)	3	0.082	(33)	3	0.076	(37)	3	189
m	127			125			121			118			115			
m/N	2.54%			2.50%			2.42%			2.36%			2.30%			

Note. [a]$d_{m,n}$, Kolmogorov-Smirnov test statistic; C_s, sensitivity class; r, rank; m, number of behavior-giving simulations; N, total number of simulations (5000); m/N, success rate.

Table 8. Median values of the marginal distribution of key input factors[a,b].

Feared endpoint						Desired endpoint					
Key input factors	Replicates					Key input factors	Replicates				
	1	2	3	4	5		1	2	3	4	5
$y_{TP:TSS}$	0.8	0.8	0.8	0.7	0.8	$y_{TP:TSS}$	0.4	0.4	0.4	0.4	0.4
τ_F	0.3	0.3	0.3	0.2	0.2	$\tau_{F,recruit}$	0.4	0.4	0.4	0.4	0.4
$\tau_{F,recruit}$	0.4	0.4	0.4	0.4	0.4	v_s	0.6	0.6	0.6	0.7	0.6
λ_Z	0.7	0.7	0.8	0.7	0.7	G	0.4	0.4	0.3	0.4	0.4
$K_{A,C}$	-.-	-.-	0.7	0.7	0.6	τ_F	0.4	0.4	0.3	0.3	0.4
τ_C	0.3	-.-	0.4	0.3	-.-	τ_H	0.4	0.4	-.-	0.4	0.3
$v_{t,mix}$	-.-	-.-	0.4	-.-	0.3	τ_M	0.7	-.-	0.6	0.7	-.-
v_s	-.-	0.7	-.-	-.-	-.-	λ_M	-.-	0.4	-.-	0.4	-.-
λ_I	-.-	-.-	-.-	-.-	-.-	λ_Z	0.6	0.6	0.7	-.-	-.-
τ_A	-.-	-.-	-.-	-.-	-.-	θ_{growth}	-.-	-.-	-.-	-.-	0.7

Note. [a]Median values are rescaled on the interval [0,1].
[b]Blank cell (-.-) indicates that the input factor is not ranked in the top 10 for the RSA replicate.

feared endpoint. However, they are replaced by the microbial loop process parameters $\{\tau_M, \tau_H, \lambda_M\}$ at the desired endpoint. The reason for this switch in dominance between the conventional grazing food chain and the microbial loop is not quite clear, but empirical evidence suggest that it exists [34]. Indeed, the role of the microbial loop in pelagic ecosystems is still a key issue of research interest in aquatic ecology [35–38].

3.4. TSDE Trees

The tree diagram in Figure 1 (the result of Rep. #3 for the feared endpoint) is an example of the ten obtained from this analysis. Table 9 presents the same tree as records of the terminal nodes, ranked in order of decreasing relative density, and a trace (from the root node) of the sequence of input factors that define each terminal node. The high-

Table 9. Terminal nodes (TN) of the TSDE tree: feared endpoint: Rep. 3[a].

TN	Relative density	#points in node	Volume [%]	Tree level [1 = root]:							
				1	2	3	4	5	6	7	8
S_{23}	**181.554**	**4**	**0.04**	**$y_{TP:TSS}$**	**τ_F**	**$K_{A,C}$**	**τ_A**	**θ_{loss}**	**$\tau_{F,recruit}$**	**$\tau_{F,recruit}$**	**τ_I**
S_{25}	**122.549**	**5**	**0.08**	**$y_{TP:TSS}$**	**τ_F**	**$K_{A,C}$**	**τ_A**	λ_Z			
S_{22}	**25.216**	**5**	**0.39**	**$y_{TP:TSS}$**	**τ_F**	**$K_{A,C}$**	**τ_A**	**θ_{loss}**	**$\tau_{F,recruit}$**	**$\tau_{F,recruit}$**	**τ_I**
S_{24}	**10.893**	**4**	**0.72**	**$y_{TP:TSS}$**	**τ_F**	**$K_{A,C}$**	**τ_A**	λ_Z			
S_{13}	**6.127**	**5**	**1.60**	**$y_{TP:TSS}$**	**τ_F**	**$K_{A,C}$**	**$t_{recruit,0}$**				
S_{20}	**5.674**	**5**	**1.73**	**$y_{TP:TSS}$**	**τ_F**	**$K_{A,C}$**	**τ_A**	**θ_{loss}**	**$\tau_{F,recruit}$**	**$\tau_{F,recruit}$**	
S_6	4.085	5	2.40	$y_{TP:TSS}$	λ_Z	$t_{recruit,0}$					
S_{27}	4.085	5	2.40	$y_{TP:TSS}$	τ_F	v_s					
S_{19}	2.723	3	2.16	$y_{TP:TSS}$	τ_F	$K_{A,C}$	τ_A	θ_{loss}	$\tau_{F,recruit}$		
S_{16}	0.681	1	2.88	$y_{TP:TSS}$	τ_F	$K_{A,C}$	τ_A	θ_{loss}			
S_{12}	0.613	2	6.40	$y_{TP:TSS}$	τ_F	$K_{A,C}$	$t_{recruit,0}$				
S_{26}	0.272	3	21.60	$y_{TP:TSS}$	τ_F	v_s					
S_7	0.204	1	9.60	$y_{TP:TSS}$	λ_Z	$t_{recruit,0}$					
S_4	0.123	3	48.00	$y_{TP:TSS}$	λ_Z						
Total		51	100.00								
High-density		28	4.56 (up to and including TN S_{20})								

Note. [a]High-density terminal nodes (HDTN) are in bold.

Table 10. Summary of RSA and TSDE results[a].

Feared endpoint						Desired endpoint					
Input factor	#HDTNs defined by input factor replicates					Input factor	#HDTNs defined by input factor replicates				
	1	2	3	4	5		1	2	3	4	5
Primary[b]						Primary[b]					
$y_{TP:TSS}$	1	7	6	9	9	$y_{TP:TSS}$	8	8	8	9	9
τ_F	8	–	6	3	7	$\tau_{F,recruit}$	8	8	–	–	9
$\tau_{F,recruit}$	7	–	3	9	1	v_s	8	6	8	8	9
λ_Z	5	–	2	9	2	G	–	2	1	3	7
$K_{A,C}$	–	1	6	–	2	τ_F	–	–	9	–	–
τ_C	–	–	–	3	1	τ_H	2	–	–	–	5
$v_{t,mix}$	–	–	–	–	–	τ_M	3	–	7	–	–
v_s	–	6	–	4	–	λ_M	3	–	–	6	–
λ_I	–	–	–	–	–	λ_Z	–	–	–	–	–
τ_A	–	–	5	–	–	θ_{growth}	–	–	–	–	2
Secondary[c]						Secondary[c]					
a_A	6	–	–	–	–	$f_{PE,undfl}$	6	–	–	–	–
y_Z	–	4	–	–	–	$t_{undfl,0}$	–	2	–	–	–
s_{TSS}	–	2	–	–	–	$t_{ovfl,0}$	–	–	7	–	–
θ_{loss}	–	–	3	–	–	τ_C	–	–	–	6	–
κ_w	–	–	–	7	–	$\tau_{G,feed}$	–	–	–	–	9
$\varepsilon_{M,H}$	–	–	–	–	5						
$K_{A,H}$	–	–	–	–	2						
#HDTN in tree	8	7	6	9	9	#HDTN in tree	8	8	9	9	9
% vol. HDTN	3.15	3.26	4.56	3.23	2.70	% vol. HDTN	9.65	11.75	10.12	13.83	8.10

Note. [a]Blank cell (–) indicates that the input factor does not feature in the TSDE tree.
[b]Top 10 input factors derived from the RSA rankings (Tables 6 and 7).
[c]Input factors correlated with the top 10 factors in the TSDE trees.

density terminal nodes (HDTNs) are determined by a ''50% rule'', which selects terminal nodes from the top of the ordered list until the cumulative sum of points just exceeds half the initial number of points. In other words, the HTDNs collectively contain at least half the number of behavior-giving (*B*) input factor sets. This rather arbitrary rule for distinguishing high- and low-density terminal nodes is applied consistently as a basis for comparing the TSDE

replicates. Its simplicity seems rather appropriate for this preliminary computational assessment, as it provides an effective tool for communicating the outcomes to stakeholders. Results of the TSDE replicates are summarized in Table 10 simply as the number of HTDNs defined by the input factors.

The key summary statistic for this analysis is the total percentage *volume* of the high-density terminal nodes, which ranges from 2.70% to 4.56% for the feared endpoint, and from 8.10% to 13.83% for the desired endpoint. Since the percentage volume of the HDTNs indicate the proportion of the densely populated regions of the input factor sampling domain, it provides a stronger indication of the likelihood of reaching the speculated endpoints than does the success rate calculated in the previous RSA procedure. Thus, beyond concurrence with the RSA results, i.e., that the feared endpoint seems less plausible than the desired endpoint, the stakeholders can also be informed that their desires for the future condition of Lake Lanier are about three times as probable as their fears. Indeed, the partitions represented by the terminal nodes of the TSDE tree provide a useful qualitative description of the distribution of behavior-giving input factors. However, it is important to note that this form of integrated assessment is founded *inter alia* on a fixed model structure, a preset sampling domain, and prescribed behavior definitions, that are often hard to justify objectively. Thus, these underlying assumptions must always be carefully considered when employing TSDE results as probabilities for quantitative risk analyses.

Table 10 shows that some of the top 10 input factors in the RSA rankings (see Tables 6 and 7), in particular, the set $\{\tau_F, \lambda_Z, \tau_{F,recruit}, v_s, y_{TP:TSS}\}$, also define high-density terminal nodes in the TSDE trees. Thus, these *primary* factors play a key role in determining the ecological behavior of Lake Lanier, both individually, as indicated by their RSA rankings, and collectively, as depicted by their positions in the TSDE trees. As discussed in Section 2.2, the sequence of input factors that define each high-density terminal node of the TSDE tree diagram represents a set of input factors that collectively interact to match the specified behavior definition. In addition, other input factors enter into the interactions at relatively high positions in the tree. These *secondary* factors include $\{a_A, y_Z, s_{TSS}, \theta_{loss}, \kappa_w, \varepsilon_{M,H}, K_{A,H}\}$ for the feared endpoint, and $\{f_{PE,undfl}, t_{undfl,0}, t_{ovfl,0}, \tau_C, \tau_{G,feed}\}$ for the desired endpoint. The composition of secondary factors also indicates behavioral differences between the speculated endpoints. For the feared endpoint, the secondary factors describe *internal* ecosystem processes only. The extinction coefficients $\{\kappa_w, a_A\}$, and settling velocity of suspended solids $\{s_{TSS}\}$, determine the degree of light penetration for phytoplankton production, while $\{K_{A,H}, \varepsilon_{M,H}, y_Z, \theta_{loss}\}$ characterize secondary production (i.e., of zooplankton and macroinvertebrates). On the other hand, the majority of secondary factors for the desired endpoint describe *external* stressors on Lake Lanier, with $\{\tau_C\}$, the growth rate-constant for macrozooplankton, being the only internal process parameter. The parameters $\{t_{ovfl,0}, t_{undfl,0}\}$ characterize the timing of density currents associated with tributary inflows to the reservoir, $\{f_{PE,undfl}\}$ controls nutrient load distribution between the epilimnion and hypolimnion in response to the tributary density currents, and $\{\tau_{G,feed}\}$ is the rate of predation by adult fish, which are conceptually exogenous to the modeled food web. Collectively, the primary and secondary input factors identify several key attributes of Lake Lanier's ecosystem, many of which are not yet well understood. In particular, sediment-nutrient interactions, microbial and zooplankton production, and the impacts of fisheries management should be issues for future scientific investigations on Lake Lanier [30]. The outcomes of such inquiry would not only contribute significantly to improved knowledge, but also enhance stakeholder perceptions of the ecological behavior of Lake Lanier.

3.5. Synthesis

RSA ranks the importance of each input factor in matching the stakeholder-derived behavior definitions, while TSDE complements this by identifying key interactions among the input factors. Table 10 represents an integration of the RSA and TSDE results for the feared and desired endpoints, which informs the ranking of corresponding ecosystem attributes (Table 11). These rankings are based solely on the RSA ranking of input factors and the number of high-density terminal nodes defined by the input factors in the TSDE trees. For the feared endpoint the key reservoir attributes (and corresponding input factors) are: (i) nutrient loading $\{y_{TP:TSS}\}$; (ii) fish production $\{\tau_F, \tau_{F,recruit}\}$; (iii) zooplankton production $\{\tau_C, K_{A,H}, \lambda_Z\}$; and (iv) sediment-water-nutrient interactions $\{v_s\}$. For the desired endpoint, they are: (i) nutrient loading $\{y_{TP:TSS}\}$; (ii) sediment-water-nutrient interactions $\{v_s\}$; (iii) fish production $\{\tau_F, \tau_{F,recruit}, G\}$; and (iv) microbial production $\{\tau_M, \tau_H, \lambda_M\}$. Such ranking of ecosystem attributes is potentially useful to resource managers in setting priorities for policy actions, and to scientists for directing the focus of future research efforts toward resolving issues of practical relevance to the stakeholders. Also, despite gross uncertainties in the behavior definitions and input factors, it is quite encouraging that the RIMME methodology is able to identify attributes of Lake Lanier's ecosystem behavior that uniquely distinguish the speculated extreme endpoints.

Table 11. Ranking of key ecosystem attributes for Lake Lanier.

Rank	Feared endpoint	Desired endpoint
(1)	Phosphorus loading	Phosphorus loading
(2)	Fish production	Sediment-water interactions
(3)	Zooplankton production	Fish production
(4)	Sediment-water interactions	Microbial production

4. CONCLUSIONS

Within the context of adaptive community learning, as proposed by Beck et al. [2], and demonstrated here in a case study of generating environmental foresight for Lake Lanier, uncertainty is most pervasive. It arises *inter alia* from: (i) incomplete scientific knowledge of the system of interest; (ii) inadequate simulation models; and (iii) poor anticipation of future events. Uncertainty has thus become the bane of model-based environmental planning and decision-making. Recently, this situation has been intensified in an emerging era of post-normal science, characterized by high decision stakes and system uncertainties, that now demands the active integration of various diverse sources of knowledge and experience [15, 39].

This study has demonstrated the utility of an inverse approach to the computational analysis of uncertainty in environmental simulation models. In conjunction with the scientific uncertainties associated with simulation modeling, value judgment was considered in a semi-qualitative fashion, it having the flexibility of being derived from a combination of empirical data, casual observations, experiences, perceptions, and imaginations of experts and lay persons. Whereas the component procedures of the RIMME methodology are similar to contemporary Monte Carlo methods, the focus of their application in this study was reversed from that of predicting the future to backcasting from the speculated future.

Indeed, the concept of backcasting has been associated with modeling in various other fields. After reviewing the philosophical, political, institutional, and methodological problems of long-term socioeconomic and resource policy modeling and forecasting, Robinson [40] stresses the need for backcasting techniques that reveal the possibility, and test the feasibility and impacts, of alternative future endpoints. Also, backcasting has been proposed in the global change sciences, as a means of reconstructing alternative past scenarios, in order to improve the anticipation of future surprise events [41].

Although the Lake Lanier case study can be considered small-scale, relative to global climate change, for example, the dimensionality of the problem (evidenced by the 94 input factors analyzed) no doubt presented a formidable challenge. This notwithstanding, the inverse approach adopted in this study has proven to be potentially beneficial to all parties involved in a participatory environmental futures assessment. In particular, the results obtained have provided information by which: (i) stakeholders' fears and hopes for the future can be corroborated or refuted; (ii) regulatory measures can be evaluated; (iii) control actions can be prioritized; (iv) the direction for future scientific research on the environment can be focused on stakeholder- and policy-relevant issues; and (v) society can be enlightened and educated about the environment in a continuous adaptive manner. Thus, the computational analysis of uncertainty has provided a middle ground for integrating stakeholder imagination with scientific theory.

ACKNOWLEDGEMENTS

This study was funded by the United States Environmental Protection Agency (EPA) Science to Achieve Results (STAR) program, Grant #R825758, under the 1998 Water and Watersheds Program. Although the research described in this paper has received such funding, it has not been subjected to any EPA review, does not necessarily reflect the views of the Agency, and no official endorsement should therefore be inferred. The authors also acknowledge an anonymous reviewer for comments and suggestions that helped improve the quality of this paper.

REFERENCES

1. Saltelli, A., Chan, K. and Scott, E.M. (eds.): *Sensitivity Analysis*. Wiley, Chichester, 2000, 475 pp.
2. Beck, M.B., Fath, B.D., Parker, A.K., Osidele, O.O., Cowie, G.M., Rasmussen, T.C., Patten, B.C., Norton, B.G., Steinemann, A., Borrett, S.R., Cox, D., Mayhew, M.C., Zeng, W. and Zeng, X.-Q.: Developing a Concept of Adaptive Community Learning: Case Study of a Rapidly Urbanizing Watershed. *Int. Assess.* 3(4) (2002), pp. 299–307.
3. U.S. Army Corps of Engineers: *Water Allocation for the Apalachicola-Chattahoochee-Flint River Basin: Draft Environmental Impact Statement*, U.S. Army Corps of Engineers, Mobile, Alabama, 1998.
4. McCarthy, J.J., Canziani, O.F., Leary, N.A., Dokken, D.J. and White, K.S. (eds.): *Climate Change 2001: Impacts, Adaptation, and Vulnerability.* Intergovernmental Panel on Climate Change (IPCC), 2001, 1032 pp.
5. Draper, D.: Assessment and Propagation of Model Uncertainty. *J. Roy. Statist. Soc. Ser. B* 57(1) (1995), pp. 45–97.
6. Stigter, J.D. and Beck, M.B.: A New Approach to the Identification of Model Structure. *Environmetrics* 5 (1994), pp. 315–333.
7. Hankin, B.G. and Beven, K.J.: Modelling Dispersion in Complex Open Channel Flows: Equifinality of Model Structure (1). *Stochastic Hydrol. Hydraul.* 12(6) (1998), pp. 377–396.
8. Osidele, O.O. and Beck, M.B.: Identification of Model Structure for Aquatic Ecosystems Using Regionalized Sensitivity Analysis. *Water Sci. Technol.* 43(7) (2001), pp. 271–278.
9. Beck, M.B. (ed.): *Environmental Foresight and Models: A Manifesto*. Elsevier, Oxford, 2002, 473 pp.
10. Beck, M.B.: Water Quality Modeling: A Review of the Analysis of Uncertainty. *Water Resourc. Res.* 23(8) (1987), pp. 1393–1442.
11. Risbey, J., van der Sluijs, J., Kloprogge, P., Ravetz, J., Funtowicz, S. and Quintana, S.C.: Application of a Checklist for Quality Assistance in Environmental Modelling to an Energy Model. In: A.E. Rizzoli and A.J. Jakeman (eds.): *Integrated Assessment and Decision Support*, Proceedings 1st Biennial Meeting, International Environmental Modelling & Software Society, 2002.
12. van der Sluijs, J.P., Potting, J., Risbey, J., van Vuuren, D., de Vries, B., Beusen, A., Heuberger, P., Corral Quintana, S., Funtowicz, S., Kloprogge, P., Nuijten, D., Petersen, A. and Ravetz, J.: *Uncertainty Assessment of the IMAGE/TIMER B1 CO_2 emissions Scenario, Using the NUSAP Method*. Report no. 410-200-104, Dutch National Research Programme on Global Air Pollution and Climate Change (Available from www.nusap.net), 2002.
13. Osidele, O.O. and Beck, M.B.: Integrating Stakeholder Imagination with Scientific Theory: A Case Study of Lake Lanier, USA. In: A.E. Rizzoli and A.J. Jakeman (eds.): *Integrated Assessment and Decision Support*, Proceedings 1st Biennial Meeting, International Environmental Modelling & Software Society, 2002.

14. Funtowicz, S.O. and Ravetz, J.R.: Science for the Post Normal Age. In: L. Westra, J. Lemons (eds.): *Perspectives on Ecological Integrity.* Kluwer Academic Publishers, The Netherlands, 1995, pp. 146–161.
15. Ravetz, J.R. and Funtowicz, S.O.: Post-Normal Science: An Insight Now Maturing. *Futures* 31 (1999), pp. 641–646.
16. Osidele, O.O.: Reachable Futures, Structural Change, and the Practical Credibility of Environmental Simulation Models. Ph.D. Dissertation, University of Georgia, Athens, Georgia, 2001.
17. Spear, R.C. and Hornberger, G.M.: Eutrophication in Peel Inlet – II: Identification of Critical Uncertainties via Generalized Sensitivity Analysis. *Water Res.* 14 (1980), pp. 43–49.
18. Spear, R.C., Grieb, T.M. and Shang, N.: Parameter Uncertainty and Interaction in Complex Environmental Models. *Water Resourc. Res.* 30(11) (1994), pp. 3159–3169.
19. Klepper, O. and Hendrix, E.M.T.: A Method for Robust Calibration of Ecological Models Under Different Types of Uncertainty. *Ecol. Model.* 74 (1994), pp. 161–182.
20. Beven, K.J. and Binley, A.M.: The Future of Distributed Models: Model Calibration and Uncertainty Prediction. *Hydrol. Process.* 6 (1992), pp. 279–298.
21. Dilks, D.W., Canale, R.P. and Meier, P.G.: Development of Bayesian Monte Carlo Techniques for Water Quality Model Uncertainty. *Ecol. Model.* 62 (1992), pp. 149–162.
22. Brooks, S.P.: Markov Chain Monte Carlo Method and its Application. *The Statistician, Journal of the Royal Statistical Society: Series D* 47(1) (1998), pp. 69–100.
23. Morgan, M.G. and Henrion, M.: *Uncertainty: A Guide to Dealing With Uncertainty in Quantitative Risk and Policy Analysis*. Cambridge University Press, Cambridge, UK, 1990, 332 pp.
24. Hornberger, G.M. and Spear, R.C.: Eutrophication in Peel Inlet – I: The Problem-Defining Behavior and a Mathematical Model for the Phosphorus Scenario. *Water Res.* 14 (1980), pp. 29–42.
25. Conover, M.J.: *Practical Nonparametric Statistics*. John Wiley, New York, 1999, 584 pp.
26. Breiman, L., Friedman, J.H., Olshen, R.A. and Stone, C.J.: *Classification and Regression Trees*. Wadsworth International Group, California, 1984, 358 pp.
27. Metropolis, N., Rosenbluth, A.W., Rosenbluth, M.N., Teller, A.H. and Teller, E.: Equations of State Calculations by Fast Computing Machines. *J. Chem. Phys.* 21 (1953), pp. 1087–1092.
28. Hastings, W.K.: Monte Carlo Sampling Methods Using Markov Chains and their Application. *Biometrika* 57(1) (1970), pp. 97–109.
29. Klepper, O. and Bedaux, J.J.M.: A Robust Method for Nonlinear Parameter Estimation Illustrated on a Toxicological Model. *Nonlinear Anal. Theory Meth. Appl.* 30(3) (1997), pp. 1677–1686.
30. Osidele, O.O. and Beck, M.B.: Food Web Modelling for Investigating Ecosystem Behavior in Large Reservoirs of the South-Eastern United States: Lessons from Lake Lanier, Georgia. *Ecol. Model.* 173 (2004), pp. 129–158.
31. Fath, B.D. and Beck, M.B.: Elucidating Public Perceptions of Environmental Behavior: A Case Study of Lake Lanier. *Environm. Model. Software* (in press).
32. Cowie, G.M., Beck, M.B., Borrett, S.R., Osidele, O.O., Parker, A.K. and Yearwood, J.: *Foresight for Lanier: A Workshop*. Technical Report, Daniel B. Warnell School of Forest Resources, University of Georgia, Athens, Georgia, 2001.
33. Box, G.E.P. and Tiao, G.C.: *Bayesian Inference in Statistical Analysis*. Addison-Wesley, Massachusetts, 1973, 588 pp.
34. Porter, K.G.: Integrating the Microbial Loop and the Classic Food Chain into a Realistic Planktonic Food Web. In: G.A. Polis, K. Winemiller (eds.): *Food Webs: Integration of Patterns and Dynamics*. Chapman and Hall, New York, 1996, pp. 51–59.
35. Azam, F., Cho, B.C., Smith, D.C. and Simon, M.: Bacterial Cycling of Matter in the Pelagic Zone of Aquatic Ecosystems. In: M.M. Tilzer, C. Serruya (eds.): *Large Lakes: Ecological Structure and Function*. Springer-Verlag, Berlin, 1990, pp. 477–488.
36. Hart, D.R., Stone, L. and Berman, T.: Seasonal Dynamics of the Lake Kinneret Food Web: The Importance of the Microbial Loop. *Limnology and Oceanography* 45(2) (2000), pp. 350–361.
37. Anderson, T.R. and Ducklow, H.W.: Microbial Loop Carbon Cycling in Ocean Environments Studied Using a Simple Steady-State Model. *Aquat. Microb. Ecol.* 26(1) (2001), pp. 37–49.
38. Hulot, F.D., Morin, P.J. and Loreau, M.: Interactions Between Algae and the Microbial Loop in Experimental Microcosms. *Oikos* 95(2) (2001), pp. 231–238.
39. van der Sluijs, J.P.: A Way Out of the Credibility Crisis of Models Used in Integrated Environmental Assessment. *Futures* 34 (2002), pp. 133–146.
40. Robinson, J.B.: Unlearning and Backcasting: Rethinking Some of the Questions We Ask About the Future. *Technol. Forecasting Social Change* 33 (1988), pp. 325–338.
41. Schneider, S.H., Turner, B.L. and Garriga, H.M.: Imaginable Surprise in Global Change Science. *J. Risk Res.* 1(2) (1998), pp. 165–185.